行政院國家科學委員會補助專題研究計畫成果報告

※※※※※※※※※※※※※※※※※※※※※※※※※
※　　　　　　　　　　　　　　　　　　　　　　　※
※　　　高層建築偏心引發振態耦合氣彈力現象　　　※
※　　　　　　　之風洞基礎研究　　　　　　　　　※
※※※※※※※※※※※※※※※※※※※※※※※※※

計畫類別：■個別型計畫　　□整合型計畫
計畫編號：NSC90－2211－E－032－010－
執行期間：90 年 08 月 01 日至 91 年 07 月 31 日

計畫主持人：鄭啟明
共同主持人：

本成果報告包括以下應繳交之附件：
- □赴國外出差或研習心得報告一份
- □赴大陸地區出差或研習心得報告一份
- ■出席國際學術會議心得報告及發表之論文各一份
- □國際合作研究計畫國外研究報告書一份

執行單位：淡江大學土木系

中　華　民　國　91 年　10 月　31 日

行政院國家科學委員會專題研究計畫成果報告

高層建築偏心引發振態耦合氣彈力現象之風洞基礎研究

計畫編號：NSC90－2211－E－032－010－
執行期限：90 年 08 月 01 日至 91 年 07 月 31 日
主持人：鄭啟明　淡江大學土木系
計畫參與人員：藍朝園 林政勳　淡江大學土木系

中文摘要

本文以氣彈力風壓模型實驗探討高層建築因振態耦合而引發的氣彈力現象。風洞實驗以模型之扭轉振態與水平振態間的頻率比為控制參數，同步量取風壓、振動與尾跡風速。研究結果顯示：頻率比是影響振態耦合氣彈力現象的重要因素。不同的頻率比決定了結構的耦合振態模式，也進一步影響了建築物所受的風力特性。

關鍵詞：氣彈力風壓模型、頻率比、振態耦合氣彈力現象

Abstract

A series of aeroelastic pressure model tests were performed on a square shaped tall building with aspect ratio of 7 in turbulent boundary layer flow. The aeroelastic pressure model is consisted of a rigid square cylinder mounted on a base pivoted spring-damping system. The pressure model was instrumented by 28 pressure taps uniformly distributed on 2/3 of the building height. During wind tunnel experiment, the wind pressure data of the 28 pressure taps were simultaneously sampled along with building's motion and wake velocity measurement at building's wake. It was found that the ratio of building's torsional natural frequency to the lateral frequency, R_f, plays a governing role on the building's vibration mode, consequently, this frequency ratio influences the acrosswind load and the wind induced vibration of tall building.

Keywords: aeroelastic pressure mode, frequency ratio, mode-coupling aeroelastic phenomenon

Introduction

Along with the economic growth and urbanization of the modern society, high-rise becoming a common practice. Besides the basic strength and safety criteria, human comfort and building serviceability gain essential roles in building design. Generally speaking, higher the building lower the building's natural frequency, more sensitive the building towards the wind actions. A slender building is more vulnerable to the excessive motion induced by vortex shedding. It is necessary to gain detail knowledge on building aerodynamics and building aeroelastics in order to be able to acquire better precision on the building's dynamic response due to wind loads.

Analytical studies on the effects of lateral/torsional coupling indicates that when the frequency ratio approach 1.0, the response at corner will increase significantly due to the presence of eccentricity. However, somewhat different phenomenon is observed in the aeroelastic model study. When the lateral and torsional mode frequencies are drawn closer, the acrosswind response near the critical velocity will unexpectedly decrease. By placing the resistance center up-stream of the mass center, instead of the response increase suggested by the structural mode coupling consideration, the acrosswind

response will decrease. It suggests that properly introducing structural mode coupling could result in favorable structural aeroelastic behavior. Full description of this aeroelastic phenomenon requires further investigation.

This research project proposes to conduct a thorough wind tunnel investigation on this special building aeroelastic phenomenon. A combination of aerodynamic and aeroelastic testing frame should be built in order to probe this problem efficiently. In short, the model should be able to behave accordance with aeroelastic similitude, while the surface pressure, wind load, dynamic motion and vortex shedding characteristics can be measured simultaneously. Then, through cross-spectral analysis, and comparison between the stationary model and the ones with mode-coupled vibration, the fundamental of this aeroelastic phenomenon can be revealed.

Experimental Apparatus

In order to investigate the insight of the wind-structural interaction, a new type of pressure model was built. The so-called aeroelastic pressure model is consisted of a rigid square cylinder mounted on a base pivoted spring-damping system.. A square cylinder with a width of 10 cm, height 70 cm, and aspect ratio H/D = 7 was chosen to represent the high-rise building. The pressure model was instrumented by 28 pressure taps uniformly distributed on 2/3 of the building height. During wind tunnel experiment, the wind pressure data of the 28 pressure taps were simultaneously sampled along with building's motion and wake velocity at building's wake. The tri-axial mechanism at base provides alongwind, acrosswind and torsional motions. It was found that the ratio of building's torsional natural frequency to the lateral frequency plays a governing role on the building's vibration mode, consequently, this frequency ratio determines the acrosswind load and the wind induced vibration of tall building. The frequency ratio, R_f , is defined as:

$$R_f = \frac{torsional \quad frequency}{lateral \quad frequency}$$

Total of 7 values of R_f were used during this study, R_f = 2.0, 1.4, 1.1, 1.05, 0.95, 0.9, 0.8. Majority of the building models have structural density of $\rho_s = 200 kg/m^3$ and 2.2% of critical damping, which corresponds to mass-damping coefficient M_D= 3.93. Another model with 3.5% of critical damping (M_D= 6.25) was used for comparison only. The blockage ratio was less than 5%; therefore, this effect was ignored. The Reynolds number was kept greater than 4×10^4 for most wind tunnel experiments.

Results and Discussion

Building's response

At the beginning of this study, the structural response of models with two different mass-damping coefficient, M_D= 3.93 & 6.25, were compared with the predictions based upon the wind loads acting on a stationary model. The frequency ratio, R_f, was set up at 2.0, so that the mode coupling effect was excluded. The alongwind mean and dynamic response of both models agrees quite well with the predicted value.. As for the acrosswind dynamic response, when the RMS response is small, i.e., $\sigma_y \le 0.03D$, the acrosswind response of M_D=6.25 model is equal or slightly less than the predicted response. For model with mass-damping coefficient M_D= 3.93, the acrosswind RMS response is well exceeding the 0.03D threshold, measured dynamic response become significantly greater than the predicted value due to the effect of negative aerodynamic damping.

Figure 1 shows the acrosswind RMS response of testing models. It clearly indicates that when the frequency ratio, R_f, approaches but greater than 1.0, the models' acrosswind response reduces significantly comparing to the case of R_f = 2.0. However, in the cases of R_f less than 1.0, the testing models steadily drift into a state of

aerodynamically unstable, their acrosswind responses increase and would well exceed the response of R_f = 2.0. The model also exhibits noticeable increase on the alongwind and torsional dynamic responses when R_f becomes less than 1.0. In short, R_f =1.0 is a critical value on the torsional/lateral frequency ratio. The square shaped tall buildings would register contrary aeroelastic characteristics when it frequency ratio falls at the opposite side of 1.0.

3.2 Wind loading

The RMS lift force coefficients of models with M_D= 3.93 and frequency ratio R_f = 2.0, 1.1, 0.9, are shown in Figure 2.. For R_f = 2.0, i.e., without the torsional/lateral coupling effect, the non-dimensional RMS lift force measured from the aeroelastic pressure model is slightly less than the stationary model except at critical wind speed. However, in the case of R_f close but greater than 1.0, the lift coefficient becomes less than the stationary model even at critical wind speed; on the other hand, when R_f becomes less than 1.0, the lift coefficient shows significant increase near critical wind speed. Similar results can be observed on the torsional force measurement and the velocity spectra measured at the wake of building model.

Based on the side face mean pressure distribution of models at various wind speed. It can be observed that, for model with frequency ratio R_f = 2.0 & 1.1, the surface pressure taken from the oscillatory models is consistently greater than the stationary model for all pressure ports, and show some pressure recovery near the rear corner. Between the two models, the R_f = 1.1 model exhibits higher surface pressure than the R_f = 2.0 model. When the frequency ratio becomes less than 10, R_f = 0.9, the model shows weaker pressure recovery at wind speed away from critical value. Near critical wind speed, $U_r \approx 10.0$, however, the oscillatory model exhibits equal or lower pressure to the stationary model. The side face RMS pressure coefficients analized in this study. Models with frequency ratio R_f = 2.0 & 1.1, show similar or lightly lower value of C'_P as the stationary model. The R_f = 0.9 model, on the other hand, shows significant increase of C'_P near critical wind speed. The base pressure coefficients, $\overline{C}_{Pb}$ & C'_{Pb}, have the similar trend. For models with frequency ratio greater than 1, R_f = 2.0 & 1.1, the mean base pressure taken from the oscillatory models is greater, and the RMS base pressure is slightly lower than the stationary model. For models with frequency ratio less than 1, R_f = 0.9, the oscillatory model has lower mean base pressure and higher RMS base pressure near critical wind speed.

A single hot film sensor, placed at 1.0 D from the leeward face and 1.5 D from the model's center line, was used to measure the wake velocity fluctuations as an indication of vortice intensity. The velocity spectra of model with frequency ratio equals to 2.0 indicates that the spectral peak gradually increases with wind speed and reaches maximum value at critical wind speed. When the frequency ratio approaches but remains greater than 1.0, the maximum of the spectral peak decreses and becomes less than the stationary condition. For the case of frequency ratio less than 1.0, the largest spectral peak can be observed.

The wake velocity, model surface pressure and the wind force coefficient data seem to suggest that, near the critical wind speed, when the frequency ratio is greater than 1, the separated free shear layer of the oscillatory model is more likely to be affected by the rear corner, weaken the wake vorticity, hence causing the increase of the on side face pressure and base pressure. When the frequency ratio becomes less than 1, the vortex shedding process is somehow enhanced by the model's oscillation, the side face and wake pressure become more negative than the stationary model.

Based upon the correlation between acrosswind and torsional motion, $R_{y\theta}(0)$, shown in Figure 3; and the correlation between pressure measurement and lateral motion, two vibration modes can be draw-up as in Figure 4. For $R_f > 1.0$, the front-end

tips toward the centerline, and the separated free shear layer is more likely to be interfered by the rear corner. When $R_f < 1.0$, the rear corner tips toward the centerline, in this case, not only the vortex shedding is better synchronized with respect to the model's motion, the free shear layer is freer to roll up and form vortices in the wake, therefore, enhance the vortex shedding process. This mode-coupling aeroelastic behavior can be further related to the beat between structural lateral and torsional modes.

Conclusions

The square shaped tall building registers contrary aeroelastic characteristics when it frequency ratio falls on the opposite side of 1.0. when the frequency ratio, R_f, approaches but greater than 1.0, the models' acrosswind response reduces significantly. However, in the cases of R_f less than 1.0, the models steadily drift into aerodynamically unstable. Two vibration modes can be draw-up. For $R_f > 1.0$, the front-end tips toward the centerline, and the separated free shear layer is more likely to be interfered by the rear corner. When $R_f < 1.0$, the rear corner tips toward the centerline, in this case, the free shear layer is freer to roll up and form vortices in the wake, therefore, enhance the vortex shedding process.

References

Cheng, C.M., Lu, P.C., Lo, H.Y., 1999, 'Acrosswind Responses of Square Shaped High-rise Buildings with Eccentricities', *Wind Engineering into the 21st Century, Proceedings of the Tenth International Conference on Wind Engineering*, Copenhagen/Denmark, pp. 631-636.

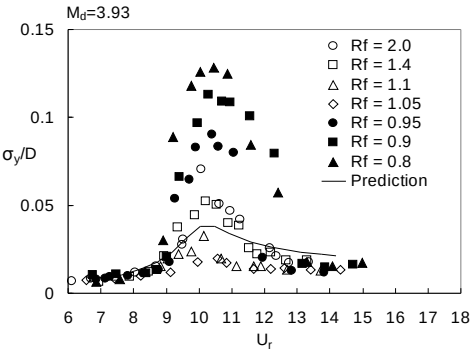

Figure 1 Acrosswind RMS response

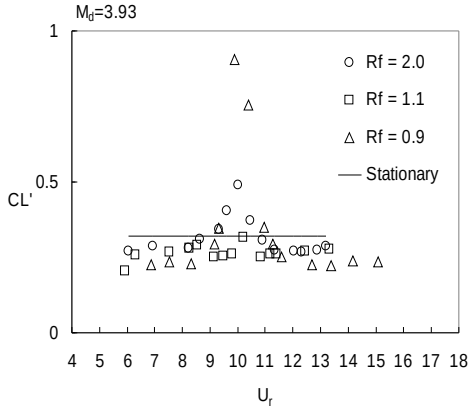

Figure 2 Lift force coefficient

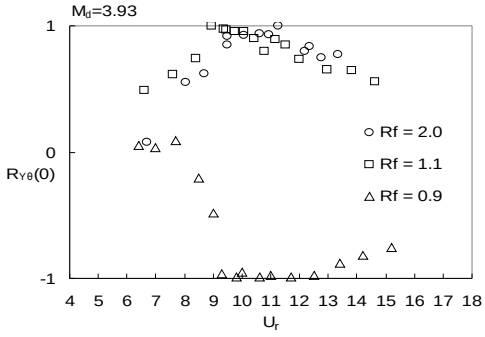

Figure 3 correlation coefficients, $R_{y\theta}(0)$

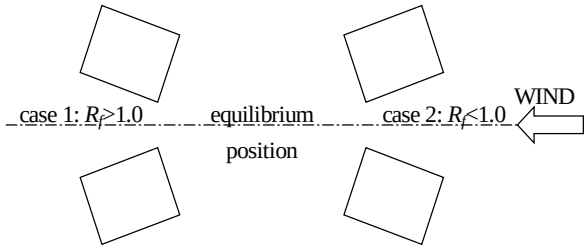

Figure 4 vibration modes under various frequency ratios

第五屆亞太風工程會議(APWECⅤ)報告

時間： 2001/10/20　至　2001/10/25

地點：日本京都

參與會議人數：參與會議者 301 人，來自 18 個國家或地區，中華民國籍 8 人。

經過：

1. 10/19 搭乘日亞航抵達東京 Narita Airport, 轉往神奈川縣厚木市之東京工藝大學。10/20 受邀參與 The Inaugural Meeting of Wind Engineering Research Center at Tokyo Institute of Polytechnics, Atsugi.並發表論文"The Effects of Deck Shape and Oncoming Turbulence on the Bridge Aerodynamics"..
2. 10/21 由 Atsugi 搭乘新幹線轉往 Kyoto 之國際會議廳參加第五屆亞太風工程會議(APWEC V), 10/21 晚上辦理報到及參加 Ice Breaker, 正式會議時間為 10/22 至 10/24。本人於 10/22 上午發表論文"Acrosswind Aerodynamic Damping of an Isolated Square Building"。10/23 中午代表台灣參加 Steering Committee, 會中議決下屆會議於 2005 年在韓國漢城召開。10/23 下午擔任 session chairman, 與 Prof. Taniike (Osaka City Univ.)共同主持 Vibration Control Session 之論文發表。
3. 10/25 於京都大學參與 2nd International Workshops on Codification for Wind Loads。10/26 經由大阪 Kansai Airport 返國。
4. 參與此次會議收益良多，在此不予詳述。

報告撰寫人：淡江大學土木系鄭啟明

Acrosswind Aerodynamic Damping of Isolated Square Shaped Buildings

C.-M. Cheng[1)] P.-C. Lu[2)] M.-S. Tsai[3)]

1) Department of Civil Engineering, Tamkang University, Taipei, Taiwan, ROC
2) Department of Water Resource and Environmental Engineering, Tamkang University
3) Center for Atmospheric Environment and Wind Engineering Studies, Tamkang University

Abstract

Systematic aeroelastic model tests were performed to study the acrosswind responses and aerodynamic damping of isolated square shaped high-rise buildings. The experimental measurements were then compared with response predictions based upon wind loads obtained from stationary pressure model. Results indicate that urban terrain flow field is aerodynamically stable for the square shaped buildings. In open terrain, buildings' responses can be categorized into three regions based on the Scruton Number: (1) region of aerodynamically stable, $\mathrm{Scr} \geq 6.28$, (2) region of aerodynamically unstable, $2.76 \leq \mathrm{Scr} \leq 5.82$, (3) region of aerodynamically divergence, $\mathrm{Scr} \leq 2.18$. Empirical models for aerodynamic damping are presented. When the aerodynamic damping is incorporated with lift force spectra, the calculated acrosswind responses show good agreement with measurements.

Keywords: aerodynamic damping, acrosswind response, square building, wind tunnel test.

Introduction

A high-rise building experiences alongwind, acrosswind and torsional vibration due to the following wind-structure interaction mechanisms: (1) incident turbulent flow, (2) wake flow, (3) motion induced force. The alongwind vibration is caused by the incident turbulence, and the response can be estimated with satisfactory accuracy by adopting the quasi-steady theory and strip theory. Acrosswind and torsional vibrations are mainly caused by the separation and vortex shedding processes of the wake flow. Quasi-steady theory no longer valid, therefore, the acrosswind and torsional motions can not be predicted accurately. As for the motion induced forces, lock-in is the most likely to occur in the case of high-rise buildings. When the amplitude of acrosswind vibration exceeds a few percentage of building width, vortex shedding frequency may stray off the Strouhal Number relationship and

synchronize to building's natural frequency for a certain range of wind speed. This lock-in phenomenon will enhance the regularity on vortex shedding process and further increase building's motion. If the aeroelastic effect is neglected and the acrosswind response is estimated solely based on lift force data from the stationary model test, it is likely to be underestimated for buildings with large aspect ratio.

Davenport & Novak [1] proposed a two-stage vibration model for vortex induced vibration, namely, random excitation and harmonic excitation stages. When building tip amplitude, in random excitation, exceeds 2% of building width, harmonic excitation takes over. Kwok & Melbourne [2], based on the aeroelastic studies in boundary layer flow, indicated that, when wind velocity does not close to the critical velocity, acrosswind response is proportional to the -1/3 to -1/2 power of structural damping, proportional to -1 power of structural damping near critical velocity. This observation verified Davenport and Novak's two-stage model. Kareem [3] constructed the acrosswind force spectra of a square shaped building through pressure measurements. During the structural response calculation, it was found that introducing aerodynamic damping leads to a better result. Matsumoto [4] used data from aerodynamic and aeroelastic tests to show that, for rectangular cylinder with 4.0 aspect ratio and cross-sectional depth/width ratio of 0.6 and 1.0, acrosswind vibration exhibited instability in a α =0.2 flow field. Hayashida et. al. [5] also showed that , for a square cylinder with aspect ratio equals to 7.5, the acrosswind motion has positive aerodynamic damping in a α =0.25 flow field. Vickery & Steckley [6] showed that, with augment of aerodynamic damping, the acrosswind response can be accurately predicted for a *H/D*=13.3 square cylinder in a α =0.112 flow field. Marukawa et. al. [7] studied the aerodynamic damping of rectangular shaped buildings in open terrain flow field, showed positive aerodynamic damping in the alongwind direction for all models, and negative aerodynamic damping in the acrosswind direction for slender buildings with small side ratio. All earlier research works pointed out the importance of aerodynamic damping on buildings' response. However, this phenomenon is yet to be systematically quantified.

In this paper, authors used aeroelastic models to study the acrosswind vibration behavior of isolated square cylinders with aspect ratio *H/D*=5,7 in boundary layer flows. Aerodynamic damping was calculated via inverse response method. Experimental measurements were then compared with calculated building responses. The wind force spectra used in the response calculation, shown in Figure 1, were obtained from pressure measurements on a stationary model with identical shape.

2. Experimental Setup

The aeroelastic tests were conducted in a boundary layer wind tunnel at

Tamkang University. This wind tunnel has an $18.0m \times 2.0m \times 1.5m$ test section. Two sets of atmospheric boundary layer flows, *BL1* and *BL2*, were generated to represent flows over open and urban terrain, respectively. *BL1*, the open terrain flow field, has a $\alpha = 0.15$ mean velocity profile, with turbulent intensity varying from 20% near ground to 3% at gradient height. *BL2*, the urban terrain flow field, has a $\alpha = 0.32$ velocity gradient with turbulent intensity varying from 35% to 6%. The gradient height is 120cm $\pm$10cm for both flow fields. During model testing, velocity at model height, U_H, was taken as the normalization factor for the reduced velocity, $U_r = U_H / f_0 D$.

Rigid body, base pivoted aeroelastic model system, shown in Figure 2, was used in this study. A dual axes mechanism was used to allow the aeroelastic model to have two sway mode vibrations. Square cylinder with aspect ratio, *H/D*, equals to 7 was chosen to be the primary geometric shape of this investigation, limited wind tunnel tests were also carried out on a *H/D*=5 model.. Model's width is kept at 10 cm. Blockage ratio is less than 5%, therefore, its effect ignored. Reynolds number was kept greater than 4×10^4 for most of the wind tunnel experiments, which is higher than $R_{e,cr} \approx 2.0 \times 10^4$ required for Reynolds number similarity.

Three structure densities, ρ_s = 151 *kg/m*^{3}, 198 *kg/m*^{3} and 231 *kg/m*^{3} were used. Structural damping, varying from 0.4% to 6%, was provided by a oil damper device at base of the aeroelastic model. The following form of mass-damping coefficient (Scruton number, *Scr*) was used as the experimental controlling parameter,

$$Scr = \frac{\int_0^H m(z)\Phi^2(z)dz}{\int_0^H \Phi^2(z)dz} \frac{\xi}{\rho D^2} \qquad (1)$$

Fifteen cases of Scruton number were used in this study.. The value of *Scr* varies from 0.59 to 10.02.

The alongwind dynamic response is mainly caused by incident turbulence. In other words, the higher the wind speed, the greater will be the structural response. Figure 3 shows measured and predicted fluctuating alongwind response of model with $Scr \cong 5.0$. In *BL1*, experimental measurements agree well with prediction for velocity less than the critical value, $U_r \le U_{r,crt}\ (\approx 11.0)$. For higher wind speed, measurements become less than the predictions. In *BL2*, the measured values are consistently less than predictions. These observations suggest that structural motion induces positive aerodynamic damping in the alongwind direction. The prediction of alongwind dynamic response based solely on wind force spectrum tends to be

conservative. The quantitative analysis of aerodynamic damping in building's alongwind vibration is excluded in this paper.

3. Acrosswind Response

3.1 Buildings in open terrain flow, *BL1*

In flow field *BL1*, the acrosswind response can be classified into three regions based on buildings' aeroelasitc behaviors.

3.1.1 *Region of Aerodynamic Stable, Scr* $\geq$ *6.28*

Figures 4 shows the R.M.S. tip acrosswind response of models with Scruton number greater than 6.28. In this region, the acrosswind response displays maximum value at critical velocity, $U_{r,cr} \approx 11.0$. At critical velocity, acrosswind response, σ_y / D, increases slightly from 2.3% to 3.2% when Scruton number decreases from 10.02 to 6.28. Comparison between measurements and predictions shows that, force spectrum from stationary model is sufficient for a satisfactory estimation of buildings' acrosswind response at velocity less than or equal to the critical wind speed. When wind speed exceeds critical value, positive aerodynamic damping occurs and acrosswind vibration suppressed. Data also shows that σ_y / D =3% is a critical value. Exceeding it, motion induced force becomes significant; response prediction based solely on stationary force spectrum is no longer conservative.

3.1.2 Region of Aerodynamic Unstable, 5.82 $\geq$ *Scr* $\geq$ 2.76

The acrosswind responses of this Scruton number region are shown in Figures 5. The comparison between experimental observations and predictions shows that, for reduced velocity less than 8.0, these two agree well. When U_r > 8.0, motion induced force starts to emerge, i.e., measured values become greater. This negative aerodynamic damping effect near critical velocity becomes stronger as Scruton number decrease. As wind speed exceeds critical value, aeroelastic effect weakens and response of aeroelastic model gradually approaches predicted value. It is also noticed that, the classic 'lock-in' phenomenon, which is reflected by a plateau of maximum response—does not occur, even in the case of model *Scr*=2.76 where the R.M.S. acrosswind response exceeds 0.1D.

3.1.3 Region of Aerodynamic Divergence, *Scr* $\leq$ *2.18*

Figures 6 shows that the acrosswind response amplitude in this region is about an

order greater than the previous two. For reduced velocity less than 10, vortex shedding prevails, i.e., measurements from aeroelastic tests equal or slightly less than predictions based on the acosswind force spectrum. When $U_r \geq 10$, significant aeroelastic phenomenon occurs. For model *Scr*=2.18 and *Scr*=1.54, structural response does not show maximum peaks as previous test cases, but increases monotonically with wind speed well exceeding vortex shedding's critical velocity. Then, buildings' response would decrease radically as vortex shedding regains control of the acrosswind motion, and again, measurements would agree with predictions. If buildings' Scruton number further decreases, galloping occurs. Buildings' acrosswind response would diverge, as shown in Figure 6(c) to 6(e).

Figure 7 shows the response spectra of model with *Scr*= 1.54. The spectra indicate that, at *Ur*=11.3, resonance occurs due to the conformity of the two frequencies. At *Ur*=15.0, the vortex shedding frequency is well separated from the structure's, however, model has larger response at this wind speed than *Ur*=11.3. In other words, for the *Scr*=1.54 model, structural response at higher wind speed is not dominated by vortex shedding but instead by galloping.

Applying Den Hartog's "galloping instability criteria", the galloping critical wind speed, U_g, can be found by letting the system's total damping equals to zero.

$$C_{Total} = 2M\omega_n\xi_s\left(1-\frac{3}{8\pi(3-\alpha)}\frac{1}{Scr}U_r A_1\right) \tag{2}$$

where C_{Total} is the system's total damping , ξ_s is structural damping and

$$A_1 = \left(\frac{dC_L(\alpha)}{d\alpha} + C_D(\alpha)\right)_{\alpha=0} \tag{3}$$

$C_D(\alpha)$ and $C_L(\alpha)$ are mean drag and lift coefficients under attack angle α. A_1 was calculated based on the measurements of $C_D(\alpha)$ and $C_L(\alpha)$ from another study. In *BL1*, $A_1 = 1.66$ and $A_1 \approx 0.0$ for *BL2*. Values of *Ug* for various aeroelastic models are listed in Table 1.

Table 1 Model's critical wind speed for galloping in *BL1*

Scr	0.59	0.89	1.18	1.54	2.18	2.76
Ur,cr	11.3	11.3	11.3	11.3	11.3	11.3
Ug	8.0	12.0	16.0	20.8	29.5	37.3

Careful examination on Figure 6(e) will show that, for *Scr*=0.59, when reduced velocity equals to 10, i.e., well exceeds critical galloping velocity, *Ug* =8.0, galloping does not occur. Measured response agrees with prediction fairly well even though σ_y / D=0.14. When reduced velocity approaches *Ur,cr*=11.0, model's response

becomes greater than predicted value due to vortex shedding resonance. When velocity increases and exceeds *Ur,cr*, the acrosswind response will grow further and motion pattern transforms to galloping. Based on the data shown in Figure 6 and Table 1, the galloping of a square building can be described as follows: *For a square shaped building, the acrosswind galloping does not happen spontaneously at critical galloping velocity, Ug. Instead, galloping is initiated by vortex shedding resonance, i.e., when vortex shedding's critical velocity, Ur,cr, is greater than galloping's critical velocity, Ug, galloping will be delayed until vortex shedding resonance happens. On the other hand, if Ur,cr is smaller than Ug, vortex shedding resonance will trigger and accelerate the galloping mechanism. However, this acceleration on galloping has its limitation. When wind speed is distant from Ur,cr and if the aeroelastic effect due to vortex shedding resonance diminishes, transition to galloping can not be sustained and the structural response return to the basic vortex shedding mode.*

3.2 Buildings in *BL2* flow field

The responses measured in *BL2* indicate that, regardless of buildings' Scruton number, acrosswind response has no peak value or resonance-then-galloping phenomenon. Figure 8 shows that, even when acrosswind response greater than the aeroelastic threshold, σ_y /D>3%, presence of high turbulence would damp the aeroelastic effect, i.e., negative aerodynamic damping will not occur in *BL2* flow field. Comparison of buildings' acrosswind responses in the two flow fields will show that, in *BL1*, buildings have larger resonant response near the critical wind speed, but when wind speed exceeds critical, *Ur>Ur,cr,* buildings in *BL2* flow field tend to have higher acrosswind response..

4. Aerodynamic Damping

Based on previous discussions, it is known that, when the R.M.S. tip acrosswind response of the square shaped building in open terrain exceeds 3% of the building width, wind-structure interaction becomes important. The concept of aerodynamic damping is commonly used to represent this complex aeroelastic phenomenon. Aerodynamic damping was evaluated by the inverse response method for its reliability. During aeroelastic tests, total damping of the vibration system consists of structural damping and aerodynamic damping:

$$\xi_T\,(\,total\,) = \xi_S\,(\,structure\,) + \xi_a\,(\,aerodynamic\,) \,.. \qquad (4)$$

At the beginning of this study, it is verified that, for building has small acrosswind response, i.e., negligible aerodynamic damping effect, the predicted response agrees well with measurement. Based on that, aerodynamic damping was then evaluated by the following inverse response approach for its reliability. First, the structural damping, ξ_s, of aeroelastic model was determined. Then the system's total damping, ξ_T, was obtained by adjusting it numerically so that the calculated response, which was based on the acrosswind force spectra, equaled to the measurement. The aerodynamic damping was taken as the difference of the two damping values.

Among the three Scruton number regions for *BL1* flow field, galloping occurs in the aerodynamic divergent region, $Scr \leq 2.18$. When that happens, it can be seen from the response time history that, the nature of building's motion switch from narrow bandwidth random to sinusoidal. In other words, during galloping, the basic form of acorsswind load is no longer stochastic as it is dominated by vortex shedding. The inverse response method, which is based on the stochastic acrosswind load, is no longer valid. Therefore, only the other two regions are included in the aerodynamic damping analysis. After obtaining aerodynamic damping for all model tests, three empirical models were established through regression analysis. The aerodynamic dampings are shown in figures 10 to 12.

(1) *BL1* flow field, $Scr \geq 6.28$

$$\xi_a = 0.06\left[1 - \exp(-0.2(U_r - 11)^2)\right] \tag{5}$$

In this aerodynamic stable region, aerodynamic damping is almost zero at critical velocity and positive elsewhere. ξ_a is primarily a function of reduced velocity only, model's Scruton number has little influence on it. Thus, only *Ur* is used as the only variable in the model.

(2) *BL1* flow field, $2.76 \leq Scr \leq 5.82$

$$\xi_a = -0.015 \exp\left[-\frac{Scr - 1.6}{10}(U_r - 11)^2\right] \tag{6}$$

In the aerodynamic unstable region, ξ_a becomes negative when *Ur* is greater than 8. Afterwards, ξ_a further decreases, and it reaches minimum value around critical velocity and causes maximum acrosswind response. Besides *Ur*, Scruton number also casts strong influence on aerodynamic damping. Therefore, Both *Ur* and *Scr* are used as variables in the empirical model.

(3) *BL2* flow field

$$\xi_a = 0.15\, U_r^{-3} \tag{7}$$

BL2 is a stable flow field for square shaped high-rise buildings. Aerodynamic damping is positive and proportional to -3 power of reduced velocity, Scruton number effect is negligible. In other words, for a square shaped high-rise building located in a large city, the acrosswind response can be conservatively estimated based solely on the wind force spectrum

Buildings' acrosswind responses were calculated by incorporating aerodynamic damping with lift force spectra and then compared with experimental measurements. Data in Figures 4, 5, 6 and 8 show that response calculation agrees well with experimental data obtained from the *H/D*=7 model. In order to further verify the validity of the proposed aerodynamic damping model, another set of aeroelastic test on the *H/D*=5 model was carried out. A simple correction method by the following formula [1] was adopted to compensate the aspect ratio effect on aerodynamic damping,

$$C^2 = \frac{(H/D)^2}{1+(H/2LD)} \tag{8}$$

in which, *L* is correlation length, equals to 3.0 for square cylinder. Then, the correction factor can be found:

$$A = \frac{C_{H/D=5}}{C_{H/D=7}} \cong 0.78$$

and,
$$\xi_a(H/D=5) = A \times \xi_a(H/D=7) \tag{9}$$

The results, shown in Figure 9, indicate the calculated responses in general match well with direct measurements.

5. Peak Factors

It is clearly shown in the response time history that, at the vicinity of critical wind speed, structural behavior is more in line with sinusoidal function than random. Which means the widely used Davenport's peak factor formula,

$$g = \sqrt{2\ln(\nu T)} + \frac{\gamma}{\sqrt{2\ln(\nu T)}} \tag{10}$$

,which is based on the narrow-bandwidth Gaussian process assumption, is no longer valid. An empirical model of one hour duration peak factor was derived from the experimental data.

$$g = 4.0 - (2.5 - 0.2S_{cr})\exp(-0.3(U_r - 11)^2) \tag{11}$$

The results are shown in Figure 10. It shows that, for models with *Scr* greater than 2.76 in open terrain flow field, measurements collapse to the proposed model at $U_r \geq 8$. The discrepancy at lower velocity range has little engineering significance, therefore, could be ignored. Figure 10 indicates that peak factor could be as low as 2.0 at critical velocity. Stick to Equation 10 would be over-conservative. for the acrosswind response *in BL2* and the alongwind response, the peak factor was found $g \approx 4.0$ which is slightly greater than Equation 10 due to the broad bandwidth nature of those signals.

6.. Conclusions

Some of the conclusions from this research are:

(1) In open terrain, the threshold for the negative acrosswind aerodynamic damping effect is σ_y / D=3%. Exceeding it, motion induced force becomes significant; response prediction based solely on stationary force spectrum is no longer conservative.

(2) The acrosswind response of a square shaped building in open terrain flow field can be classified into three regions: aerodynamic stable region ($Scr \geq 6.28$), aerodynamic unstable region ($2.76 \leq Scr \leq 5.82$) and aerodynamic divergence region ($Scr \leq 2.18$).

(3) For a square cylinder, acrosswind galloping will not occur spontaneously, it has to be leaded by vortex resonance.

(4) Urban terrain flow field is aerodynamic stable for square cylinder.

(5) Empirical models of aerodynamic damping are established based on experimental data. Incorporating with lift force spectrum from stationary model, building's acrosswind response can be accurately predicted.

(6) For the acrosswind response in *BL1*, the peak factor can be as low as 2.0 at critical velocity. An empirical model is proposed for better accuracy on this parameter.

References

[1] Davenport, A.G., Novak, M., 1976, Vibration of Structures Induced by Wind, Shock and Vibration Handbook, McGraw Hill.

[2] Kwok, K.C.S., Melbourne, W.H., 1981, Wind Induced Lock-in Excitation of Tall Structures, Journal of Structural Division, ASCE, Vol.107, No.ST1, pp.57-72.

[3] Kareem, A., 1982, Acrosswind Response of Building, Journal of Structural Division, ASCE, Vol.108, No.ST4, pp.867-887.

[4] Matsumoto, T., 1986, On the Acrosswind Oscillation of Tall Buildings, Journal of Wind Engineering and Industrial Aerodynamics, 24, pp.69-85.

[5] Hayashida, H., Mataki, Y., Iwasa, Y., 1992, Aerodynamic Damping Effects of

Tall Building for a Vortex Induced Vibration, Journal of Wind Engineering and Industrial Aerodynamics, 41-44, pp.1973-1983.

[6] Vickery, B.J., Steckley, A., 1993, Aerodynamic Damping and Vortex Excitation on an Oscillating Prism In Turbulent Shear Flow, Journal of Wind Engineering and Industrial Aerodynamics, 49, pp.121-14.

[7] Marukawa, H., Kato, N., Fujii, K. and Tamura, Y., 1996, Experimental Evaluation of Aerodynamic Dmping of Tall Buildings

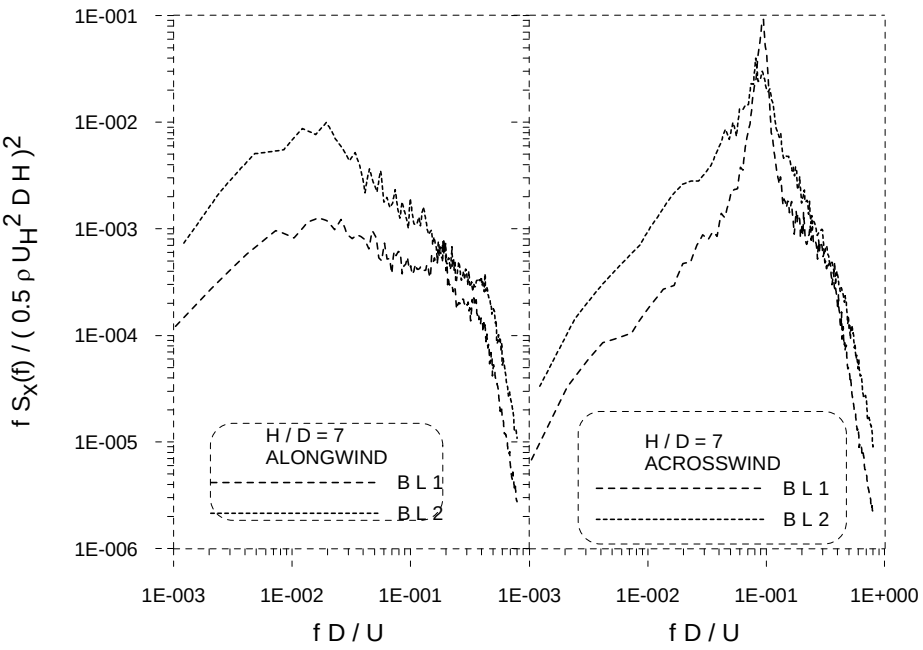

Figure 1. Force spectra of stationary model

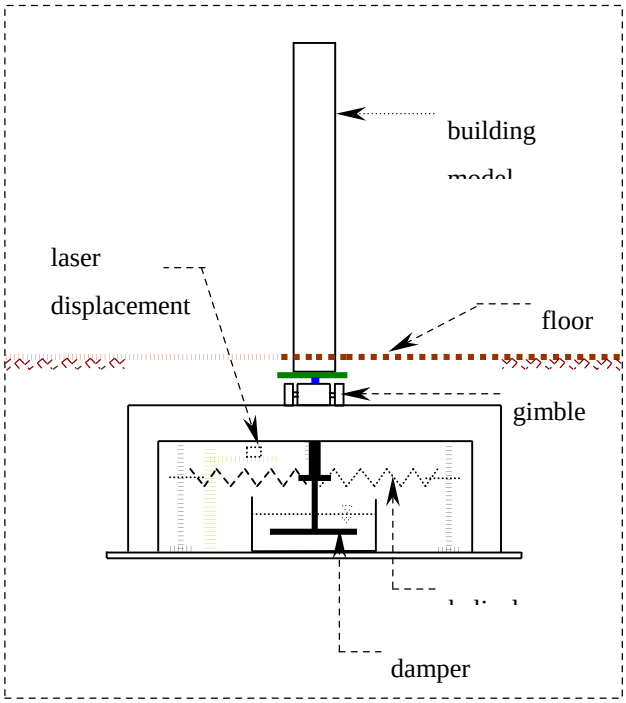

Figure 2. Aeroelastic model

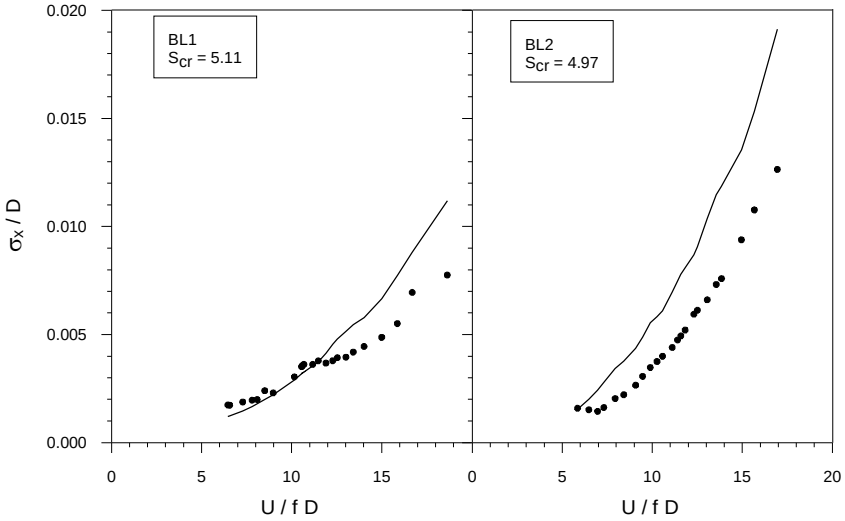

Figure 3. R.M.S. of alongwind response in BL1 , Scr 5.0

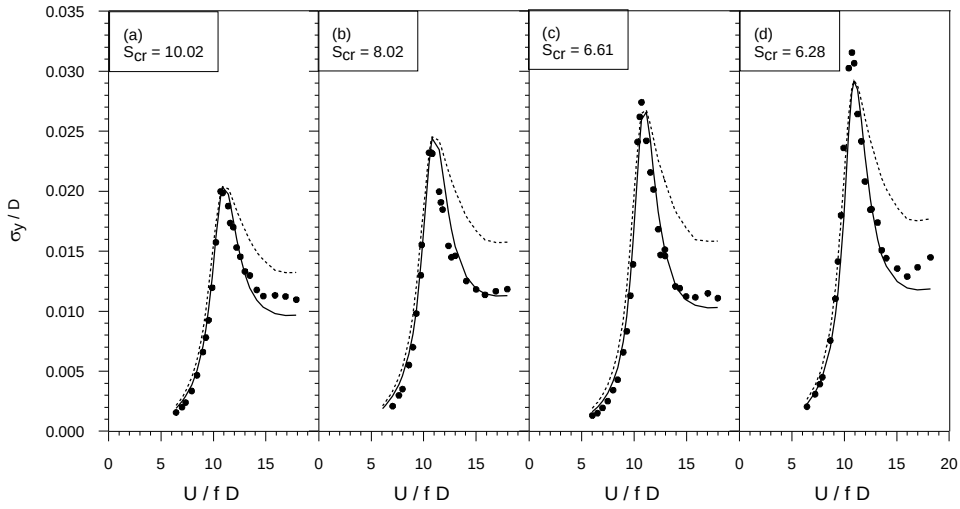

Figure 4. Measured and predicted acrosswind response in BL1—region of aerodynamic stable

●: measured

-- : prediction based on force spectra

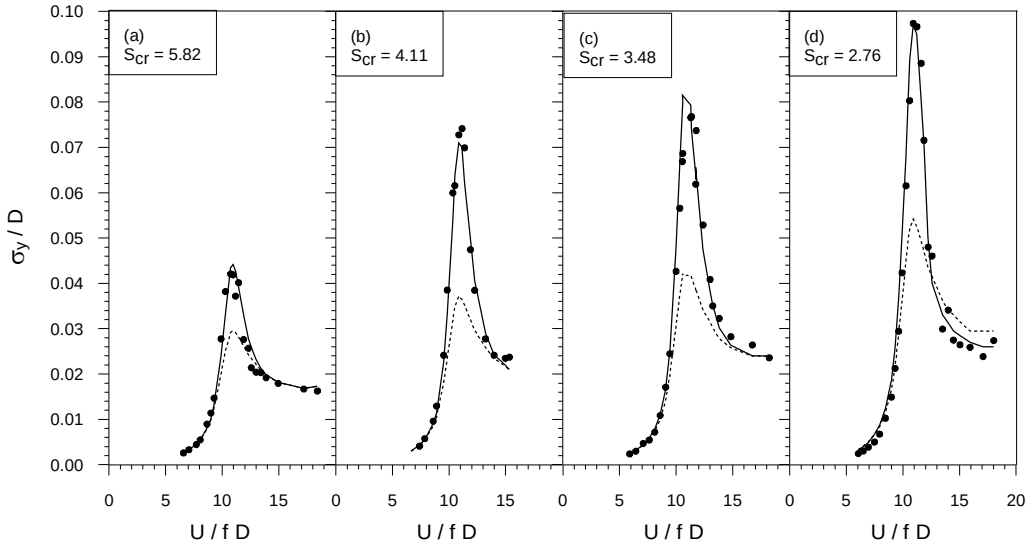

Figure 5. Measured and predicted acrosswind response in BL1—region of aerodynamic unstable

●: measured

-- : prediction based on force spectra

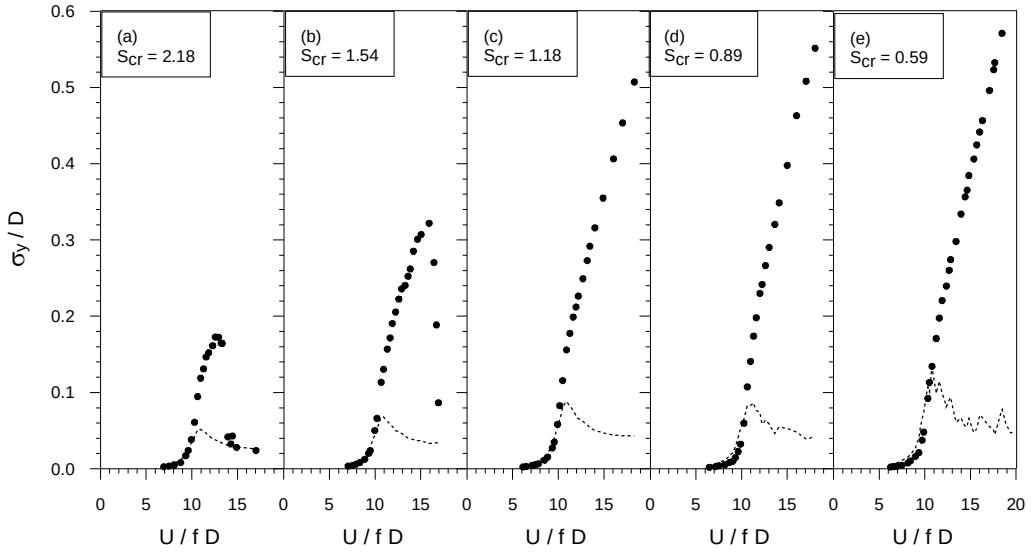

Figure 6. Measured and predicted acrosswind response in BL1—region of aerodynamic divergency

●: measured

-- : prediction based on force spectra

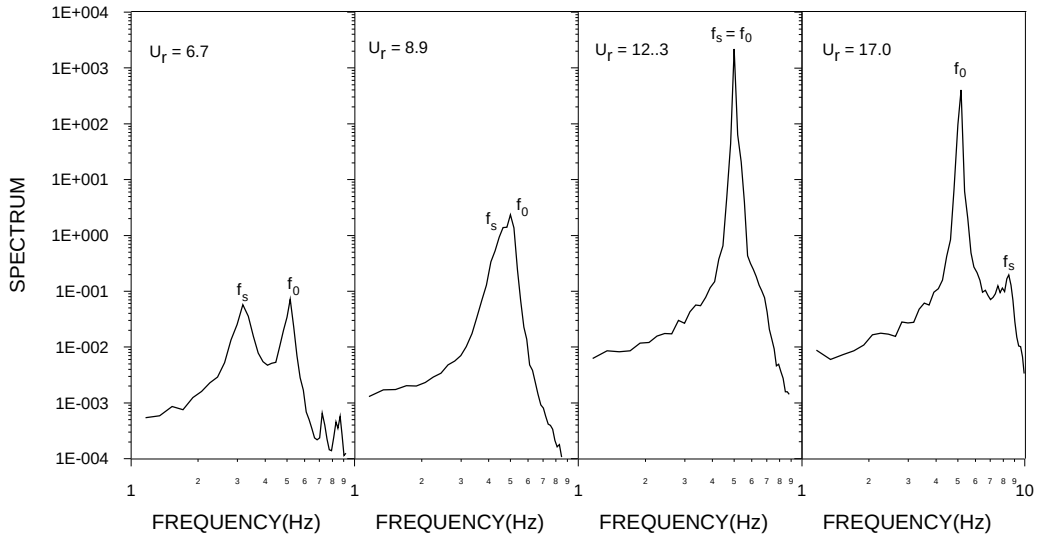

Figure 7. Power spectral densities of acrosswind responses, Scr=1.54

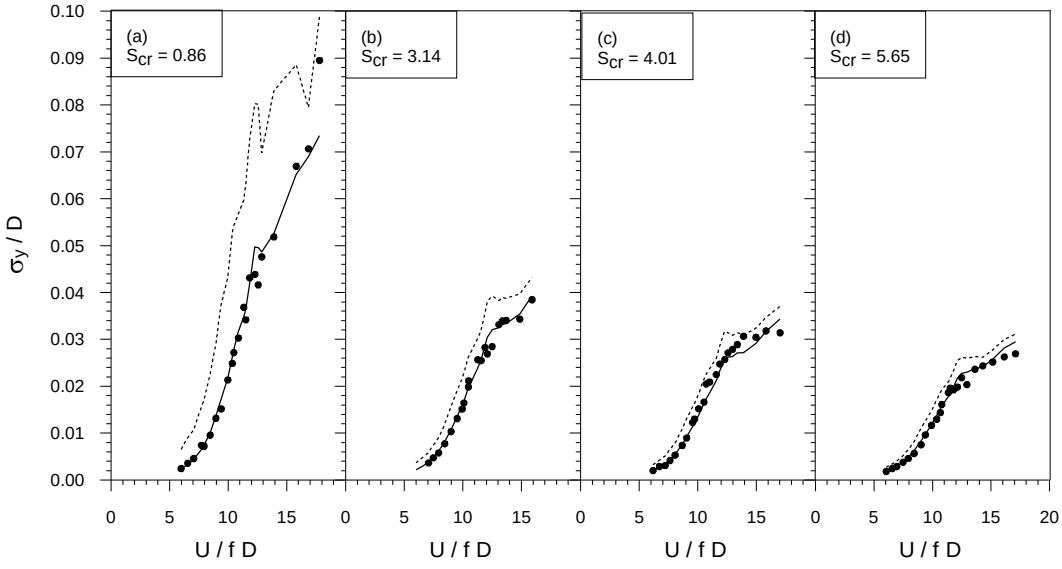

Figure 8. Measured and predicted acrosswind response in BL2

●: measured

-- : prediction based on force spectra

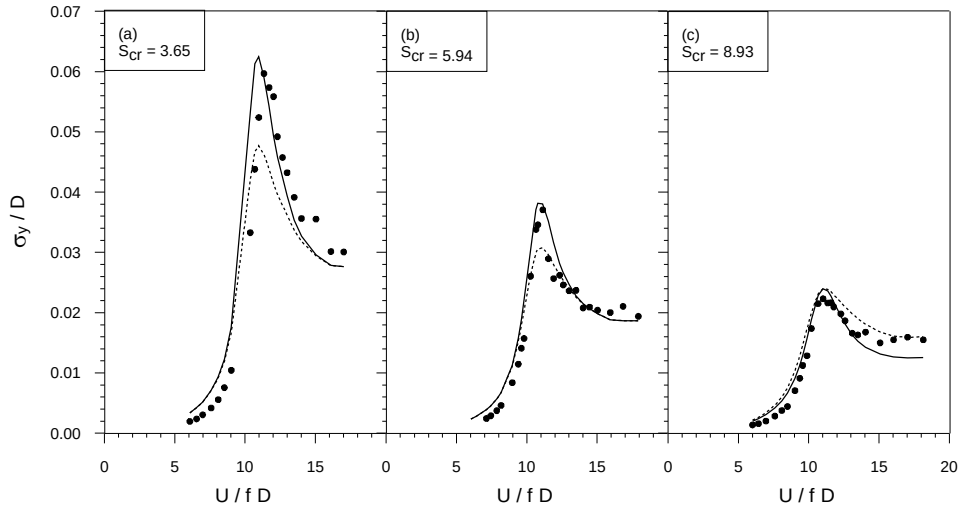

Figure 9. Measured and predicted acrosswind response of model with H/D=5, in BL1

●: measured

-- : prediction based on force spectra

—: aerodynamic damping incorporated in predicted model

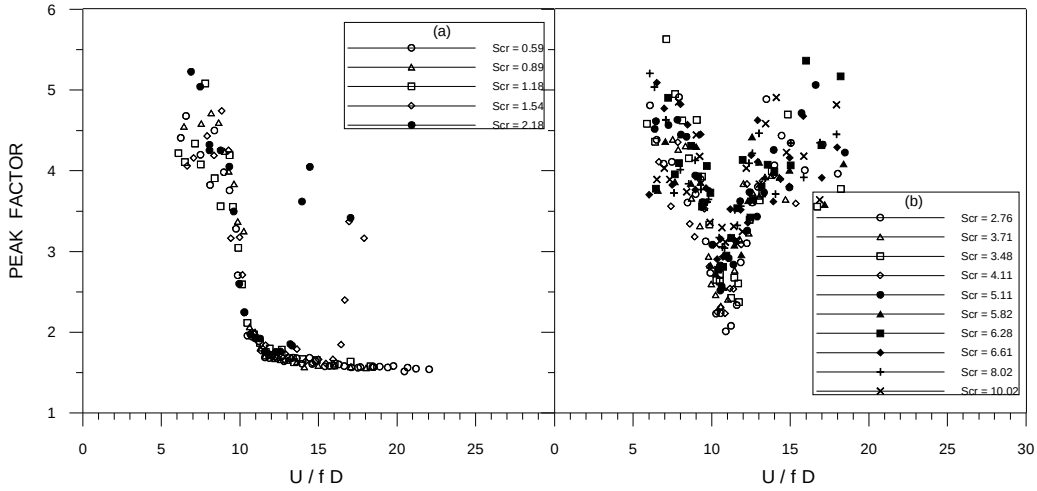

Figure 10. Peak factors of acrosswind response in BL1, (a) region of aerodynamic divergence, (b) region of aerodynamic stable and unstable